Journal of *Marine Science and Engineering*

MDPI

Article

New Insights into Tyrrhenian Sea Warming and Heat Penetration through Long-Term Expendable Bathythermograph Data

Tiziana Ciuffardi [1,*], Nadia Lo Bue [2], Giancarlo Raiteri [1], Salvatore Marullo [3] and Vincenzo Artale [2,3]

[1] Agenzia Nazionale per le Nuove Tecnologie, l'energia e lo Sviluppo Economico Sostenibile (ENEA)-Centro Ricerche Ambiente Marino Santa Teresa, 19032 La Spezia, Italy
[2] Istituto Nazionale di Geofisica e Vulcanologia (INGV), 00143 Rome, Italy
[3] Consiglio Nazionale delle Ricerche - Istituto di Scienze Marine (CNR-ISMAR), 00133 Rome, Italy
* Correspondence: tiziana.ciuffardi@enea.it

Abstract: The warming trend of the Mediterranean region is already well known, but there is still a lack of information on its seasonal/annual to multidecadal time scales and its distribution in all water masses, including deep water. New temporal and spatial evidence of this thermal variability has been presented in the Tyrrhenian Sea, thanks to twenty-year continuous monitoring by eXpendable BathyThermographs (XBTs) along a fixed route from Genoa to Palermo. The Tyrrhenian Sea is one of the deepest Mediterranean sub-basins (with a maximum depth of about 4000 m), but its interaction with neighbouring basins is controlled by topographical factors, such as the Sardinian Channel to the south and the Corsican Channel to the north. The way in which the warm signal, originating from the Levantine sub-basin, and entering from the south, affects the entire Tyrrhenian Basin spreading rapidly northwards is studied, considering its peculiarities, such as topography, surface circulation, and strong stratification, as well as its climate variability. The warming trend observed for the Tyrrhenian Sea is consistent with the trend for the Mediterranean Sea as a whole. However, the Tyrrhenian Sea shows some peculiar features: around 2014, a shift to a new equilibrium (warmer) state was detected, with mean values along the monitored route that were significantly higher than the previous period (from 1999 to 2013), especially for the subsurface level, from 100 to 450 m depth.

Keywords: XBT measurements; ocean observing systems; Mediterranean Sea; Tyrrhenian Sea; ocean water masses; climate change

Citation: Ciuffardi, T.; Lo Bue, N.; Raiteri, G.; Marullo, S.; Artale, V. New Insights into Tyrrhenian Sea Warming and Heat Penetration through Long-Term Expendable Bathythermograph Data. *J. Mar. Sci. Eng.* **2024**, *12*, 1756. https://doi.org/10.3390/jmse12101756

Academic Editors: João Miguel Dias and Mª Teresa de Castro Rodríguez

Received: 31 July 2024
Revised: 19 September 2024
Accepted: 23 September 2024
Published: 4 October 2024

1. Introduction

Several studies strongly confirm the importance of the Mediterranean Sea as a perfect natural laboratory for studying oceanographic processes and monitoring the local/regional impact of climate change [1–3]. As a marginal "sea in the middle of the land" (literally from Latin), the general circulation pattern of the Mediterranean Sea is well studied due to its specific oceanographic characteristics. Indeed, among the Mediterranean-type climates existing on the western edges of five continents, usually defined by temperate, wet winters, and hot or warm dry summers, the Mediterranean is the only one in which air–sea interaction plays a relevant role in the production of intense water transformation and deep water formation [4,5].

Moreover, the warming trend is a well-known feature of the Mediterranean region, a climate hotspot warming 20% faster than the global average [1,2,6–8]. Each year, the Mediterranean Sea reaches new records of seawater warming [9], with heat penetrating deeper into the ocean column over time. In the broader understanding of Mediterranean warming [10–14], this paper, based on synoptic and long-term observations, provides evidence of the warming signal reaching the deep layers (800 m) of the Tyrrhenian Sea, along with significant subsurface warming and intensified stratification.

The Tyrrhenian Sea (TYS hereafter) is a sort of nested laboratory itself: a semi-enclosed sub-basin in a marginal sea where the literature has shown interesting scientific questions

related to wind-driven surface circulation features, strong stratification, and mixing processes involving the entire water column, including the abyssal layer [15–18]. For example, the thermohaline staircase system, due to double diffusion in the salt finger regime, is a specific and relevant feature of this sub-basin [19]. These peculiarities, including topographical ones, make the TYS a particularly important site for assessing warming trends [20]. As reported by [21], the surface temperatures in the TYS have been rising at an average rate of 0.037 °C/y over the last 39 years, particularly during the warm seasons. As a result, the warm summer months are starting much earlier and lasting longer, making cold spells less common and less severe, while marine heatwaves have increased in frequency, severity, and duration [21,22].

The idea of this paper is to show how the TYS, at the local/regional scale, is contributing to the warming trend of the whole Mediterranean Sea by acting as a heat sink.

This paper is organised as follows: a brief description of the experimental area and dataset and of the methodology used in the analysis is illustrated in Section 2. In Section 3, the profiles' features along the transect are analysed and the seasonal and interannual thermal variability is discussed together with the ocean heat content (OHC) and sea surface temperature (SST) variability across the TYS. After the Discussion in Section 4, conclusions and directions of future work are drawn in Section 5.

2. Materials and Methods

2.1. The Study Area

In the context of this paper, we focused on the TYS, which is characterised by a complex bottom bathymetry, and is one of the deepest areas in the Mediterranean (about 4000 m). This bathymetry is a key factor influencing the TYS thermohaline circulation [23]. The circulation is constrained by three main entrances: the Corsican Channel to the north, the Sardinian Channel to the south, and the Bonifacio Strait, which, although considered less significant for the thermohaline circulation, plays a role in wind circulation [24]. To the north, the exchange with the Ligurian Sea occurs through the narrow and shallow (about 400 m depth) Corsican Channel. To the south, the TYS is connected to the western Mediterranean Sea, particularly the Provençal Basin, via the large and deep Sardinian Channel (more than 200 km long and with a maximum depth of 2000 m at the south-eastern corner of Sardinia). Additionally, the TYS communicates with the eastern Mediterranean Sea through the shallower Sicilian Strait (about 400 m average depth).

This sub-basin's morphological configuration allows the water column of the TYS to be ventilated by different water masses from both the eastern and western Mediterranean (e.g., [18,25–29]). This makes the TYS a buffer oceanic region where local water masses mix with those advected from remote areas, creating new water masses that then recirculate in the western Mediterranean. This process influences the general circulation and the formation of the deep water in the Gulf of Lion ([30] and Figure 1).

The general circulation of the TYS is also strongly influenced by wind stress, which creates a permanent cyclonic circulation along the sub-basin's coast [31]. This influence also leads to a quasi-permanent cyclone–anticyclone system (Bonifacio dipole gyre) and two seasonal anticyclones, the Central and Sicilian anticyclones, as reported in panel a) of Figure 1 (see also [15,29,32]).

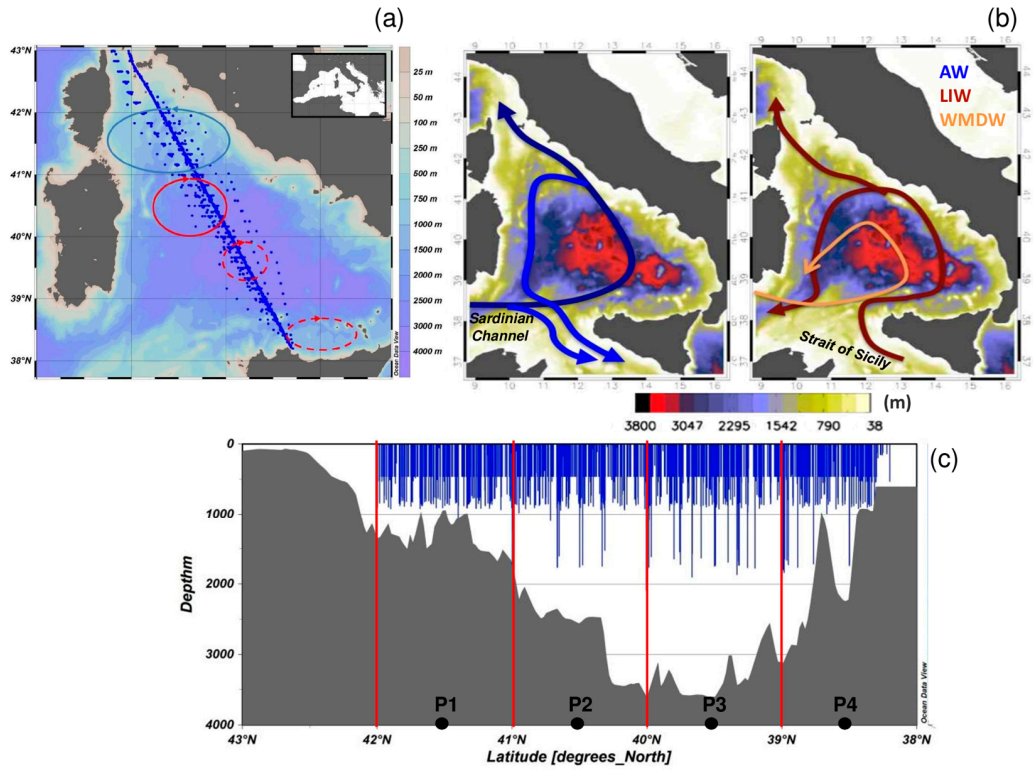

Figure 1. The transect across the Tyrrhenian Sea, from Genoa to Palermo. The upper panel (**a**) presents the domain interested by the transect, with the corresponding bathymetry, and a schematic drawing of the main vortices present in the area. Blue dots represent the locations of the XBT measurements (1999–2019) analysed in this paper. Panel (**b**) shows the main circulation patterns together with the water mass distribution of the Tyrrhenian Sea (from surface to bottom: Atlantic Water (AW); Levantine Intermediate Water (LIW), and Western Mediterranean Deep Water (WMDW), as described, among others, by [16,18,24,25]. Bathymetry along the XBT track is also shown in the lower panel (**c**) (with a resolution of 0.02° latitude) using values from the European Marine Observation and Data Network (see http://portal.emodnet-bathymetry.eu/mean-depth-full-coverage, accessed on 30 July 2024). Relevant topographic features, related to submarine mountains, and the four areas identified by their central points (P1–P4) and selected for the anomaly temperature computations are also shown.

2.2. The Experimental Datasets

In September 1999, within the European project MFS (Mediterranean Forecasting System), a monitoring project of the Mediterranean Sea began, based on the launch of XBT probes from commercial ships within a Ship of Opportunity (SOOP) programme. One of these monitoring transects is still operational on the route from Genoa to Palermo (Figure 1a) and has contributed to the collection of more than 4000 temperature profiles over the last 20 years [15,33,34]. This line is particularly relevant because it substantially coincides with the projection of track 44 of the altimetric satellites (initially TOPEX/Poseidon, then the Jason family), essential for monitoring the dynamics associated with the TYS sub-basin circulation at several space and temporal scales from the mesoscale to the basin-scale range [35]. From this large database, 2123 temperature vertical profiles over the TYS have been selected according to the procedure described in Section 2.3 for the period from 1999 to 2019 and analysed in the present investigation (see Table 1). The verified datasets are also available in the SeaDataNet portal (https://cdi.seadatanet.org/search, accessed on 30 July 2024) and in the World Ocean Database (https://www.ncei.noaa.gov/access/world-ocean-database-select/dbsearch.html, accessed on 30 July 2024). The analysed XBT probes were developed and manufactured by Lockheed Martin Sippican Inc. They can reach different maximum depths according to the model: up to about 550 m, 900 m, and 1800 m for the

T4/T6, T7/DB, and T5/T5-20 probes, respectively [36]. The speed of the ship during the navigation affects the maximum depth that the probes can reach, making it decrease as speed grows. Profiles from before 2004 were collected exclusively with the shallower XBT versions that reached a maximum depth of 450 m (green shadow cells in Table 1), then a mix of probes was used according to the bathymetry, attempting to observe some phenomena in particular areas (Figure 1c). The same database, associated with altimeter observations, has allowed us to characterise and describe the variability of recurrent surface circulation features in the area and also supported the investigation of the Tyrrhenian Intermediate Water (TIW) [15,33].

Table 1. Number of analysed XBT profiles in the Tyrrhenian Sea (42° N–38° N): 2123 profiles were analysed for the period. Black dots correspond to experimental transects. The number of profiles per month/year is reported in the last row/column. Green shadow cells represent profiles for which only the shallowest models of XBTs are available.

Year	Month												XBTs/y
	Jan	Feb	Mar	Apr	May	June	Jul	Aug	Sep	Oct	Nov	Dec	
1999									•	•	•	••	93
2000	••	••	••	••	••	•		••	•	•	•	•	293
2001													0
2002													0
2003													0
2004					•			••	•	••	•	•	164
2005	•	•	•	•	•	•			•	•	•	•	175
2006					•					•			71
2007													0
2008													0
2009													0
2010							•					•	15
2011			•			•		••				•	82
2012			•		•		•		•				85
2013	•		•		•				•			•	150
2014		•		•		•		•	•	•		•	143
2015		•	•		•	•	•		•	•		•	235
2016	•		•		•	•			•	•		•	208
2017	•		•		•				•	•		•	178
2018	•		•		•	•			•			•	177
2019	•		•										54
XBTs/month	201	88	258	84	262	219	55	87	295	218	70	286	**2123**

There are some gaps in time coverage (mainly before 2010) and the vessel's route experienced minor course changes due to the sea conditions in the earlier period and a planned variation by the shipping company after spring 2015. Since July 2010, the acquisition system has been calibrated by a test canister working at two reference temperatures. This control procedure was repeated twice during each shipping campaign, immediately before the first XBT launch and immediately after the last launch. Then, an algorithm was applied to the dataset, considering the time drift in the temperature values read at the beginning and at the end of the XBT deployments, combined with a further linear correction as a function of the deviation from the reference temperature values. More details about the correction applied to the profile data can be found in [34,37]. To further discuss underlying uncertainties, potentially related to XBT bias correction methods, XBT measurements along the Genoa–Palermo transect were verified, comparing their values in

terms of temperature–depth profiles, with those provided by Argo floats quasi-collocated in space (position differences similar to the local Rossby radius) and time (1-day time window). The differences between the two datasets have been shown by [37], considering quasi-collocated and quasi-simultaneous measurements: XBT temperature profiles collected in the TYS were proven to be in line, from a metrological point of view, with data recorded by Argo profilers. The comparison shows that agreement below 100 m depth is very consistent. XBT values have, in fact, a mean positive bias of 0.05 °C with a standard deviation equal to 0.10 °C, regardless of the specific type of XBT (i.e., fully compatible with the accuracy declared by the manufacturers). Hence, in the present analysis, the criterion of significance to be able to speak of a trend is to observe a variation over time that is greater than 2 × 0.1 °C at the same depth and for depths beyond 100 m (i.e., assuming conservatively total correlation between temperature measurements).

The fact that the Argo and CTD data are comparable to those of the XBT again supports the use of equi-spatially distributed XBT profiles in the present analysis (Table 1), especially considering that Argo floats and CTD profiles along the route are only publicly available from 2004 and, in general, the number of available CTD profiles in the TYS is extremely low. However, the available Argo data from 2004 to 2019 were extracted from the SeaDataNet portal (https://cdi.seadatanet.org/search, accessed on 30 July 2024), corroborating XBT information and integrating salinity information to trace water masses' evolution in space and time, ultimately strengthening our analysis and conclusion. To further discuss underlying uncertainties, and to provide more quantitative results on characteristics and drivers of the observed changes, sea surface temperature (SST) variability and trends within the Mediterranean Sea were analysed over the last 40 years (1982–2022) by using a satellite-based dataset from the E.U. Copernicus Marine Service Information (CMEMS). SST fields were processed and extended as described in [1].

Here, we will further examine all these datasets, looking in more detail at the vertical temperature variability and OHC, with a focus on the TYS.

2.3. Setting of the Area

The XBT data analysed were all included in a band of about 100 km of width, centred on the TYS section of the Genoa–Palermo transect. This transect crosses all the main circulation features of the TYS (Figure 1a), as described by [15], and is an area with a remarkable feature: a "V-shaped" topography confined by two platforms, the northern one more extended and the southern one limited by the Sicily shelf (Figure 1c). This complex bottom morphology influences ocean circulation by directing ocean flows and representing a barrier to the spreading of deep ocean masses, except for its deep passages; indeed, the Sardinian Channel permits the exchange of almost all water mass until 2000 m, while the Corsican Channel permits the exchange only of the AW and LIW (see Figure 1 and [23,38,39]). Figure 1 shows the bathymetry of the ocean floor of the TYS. Panel c) of this figure, where the experimental data are shown in blue, highlights the missing information for the TYS. Specifically, for XBT data, and indeed for most other probes as well, there are no measurements available to study the dynamics below 2000 m. Four different areas, identified by their central points P1-P4, were selected in the present study as being more representative of data coverage, bathymetry, and quasi-permanent circulation features (Figure 1a–c)): in the Northern TYS, where the permanent Bonifacio cyclone typically extends (centred around 41.5° N 11.0° E); in the Central TYS, characterised by the Bonifacio anticyclone (centred around 40.5° N 11.6° E); in the Central southern TYS, where the depth is greater than 2000 m and the Central anticyclone circulation takes place (centred around 39.5° N 12.4° E); and in the southern TYS (centred around 38.5° N 13.2° E), bordering the western side of the Sicilian anticyclone. The four areas were centred around the latitudes and longitudes selected above, taking into account the low value of the Rossby radius in the Mediterranean, which varies from 5 to 12 km [40]. A similar approach has also been followed by [41] and serves as a reference for comparison in the present analysis.

Finally, for each of the four points, data were analysed and presented according to four vertical layers, where available, considering the core depths of the different water masses of the TYS [31]: 10–100 m, 100–450 m, 450–800 m, and 800–1500 m (the latter being available for the deepest part of the TYS and for the XBT T5 probes). The number of XBTs resulting in the present analysis is shown in Table 2, according to water level and point distribution. Argo data, from 2004 to 2019, were extracted from the SeaDataNet portal and integrated in the present analysis, following the same approach, and considering the same four areas and their central points P1-P4. Note that data from 2010 to 2013 have not been included, as they are missing in the data portal for the selected areas.

Table 2. Number of XBTs according to the four selected points and the four water depth (WD) levels. NA stands for not applicable.

WD (m)	#XBTs			
	P1	**P2**	**P3**	**P4**
10–100	179	207	227	219
100–450	169	197	223	204
450–800	80	118	131	98
800–1500	NA	21	50	NA

2.4. Baseline for Anomaly and OHC Calculations

The subsurface temperature variations are expressed as the vertical integral of the potential temperature (°C m) following the methodology of the Copernicus Climate Change Service Report [13,42] in consistency with [43,44]. Assuming this, the traditional OHC definition in each layer of thickness $\Delta z = z - z_0$ is given by the following integral:

$$OHC_{\Delta z}(x, y, t) = \rho c_p \int_{z_0}^{z} T(x, y, z, t) dz \quad (1)$$

where ρ is the mean density and c_p is the heat capacity of seawater (assumed, respectively, to be equal to 1030 kg/m^3 and 3980 J/kg °C, from [45]).

Temperature anomalies were defined as the deviation from the reference period 1999–2019, assumed here as the baseline. The results are represented as time series anomalies per layer (±standard deviation in dashed lines). A linear trendline and corresponding R-squared were applied, as a best-fit straight line, to the OHC anomaly datasets only for the 100–450 m and 450–800 m layers during the 2010–2019 period.

3. Results

Data analysis was limited to the 10–1500 m depth range, focusing on the intermediate and deep levels. Hereafter, the results for the four selected areas, defined in the previous section, with a latitude between 38.5 °N and 41.5° N, will be reported.

3.1. Temperature Trends and Anomalies

The Hovmöller diagrams can provide useful information about the temperature variability across the water column. In Figure 2, we display the vertical sections associated with the four selected areas (referred in Figure 1c as P1–P4), drawn by the Ocean Data View software version 5.6.5 [46], along all the available transects and the 10–1500 m depth range. According to the bathymetry (Figure 1), the layers below 800 m are represented only for the central part of the sub-basin. Figure 2 shows the temporal sequence resulting from December 1999 to March 2019 across the different zonal sections. To better visualise phenomena and trends, data were grouped according to the main water mass distribution known for the TYS [28], assuming AW for the 0–200 m layer, LIW for the intermediate layer (200–800 m layer), and WMDW for the 800–1500 m layer.

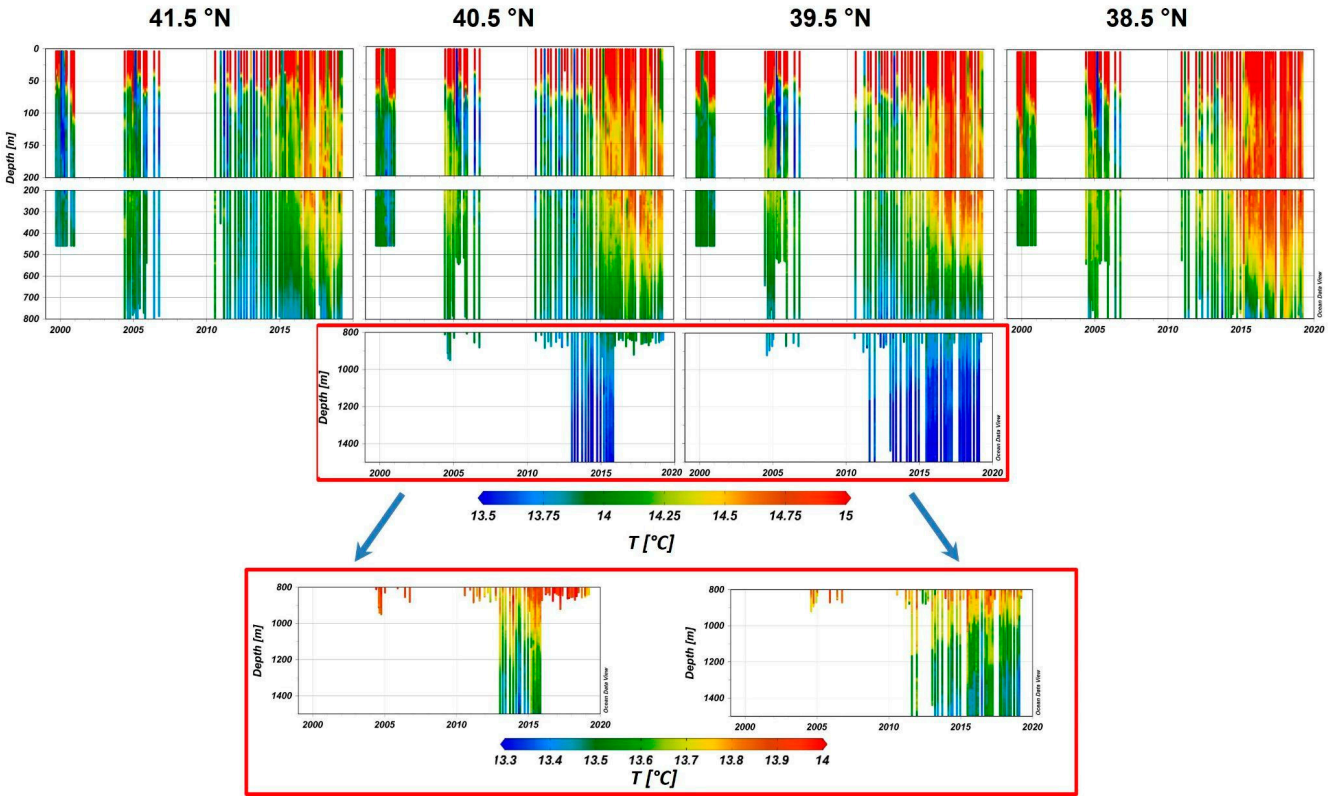

Figure 2. Hovmöller diagrams of temperature for the layer 10–1500 m along all the available XBT measurements. The sections reproduce the transect from North (left) to South (right). The deepest data are reported only for the latitudes 40.5° N and 39.5° N. For these latter, a different temperature scale (from 13.3 °C to 14 °C) has been reproduced in order to facilitate visual comparison, as shown by blue arrows. Please note that the deepest part has been zoomed using a different vertical scale.

The upper layer is generally characterised by high frequency variability and governed by the air–sea interaction that drives the seasonal cycle of thermocline depth. The seasonal effect changes over time, significantly impacting subsurface ventilation and erosion of the thermocline, particularly during the transition to winter. In all the sections, colder periods (i.e., vertical blue lines) correspond to the winter season (particularly March), when strong vertical mixing occurs. This mechanism also varies spatially; it is more pronounced in the northern part of the Tyrrhenian Sea due to its topographic and circulation characteristics (i.e., coherent cyclonic and shallow circulation in the North, versus predominantly anticyclonic and circulation in the South). Around 2014, this scenario changed significantly, with marked warming affecting the upper 400 m in the North and the upper 800 m in the basin's southern part. These temperature differences over time, at the same depth, exceeding 0.1–0.2 °C, underscore the significance of the trend detected by XBT temperature measurements. After 2018, a new scenario emerged, characterised by a temperature decrease extending into early 2019.

The deepest layer (i.e., 800–1500 m) was investigated only in P2 and P3 (i.e., centred around the latitudes 40.5° N and 39.5° N, respectively) due to bathymetric constraints. A different temperature scale, ranging from 13.3 °C to 14.0 °C, was also reproduced (bottom part of Figure 2), to facilitate visual comparison of the deepest variations. Obviously, in the deep layers the temperature anomalies are slightest in comparison with those observed in the surface and subsurface layers; however, a positive warming trend is still evident from 1200 m to 1500 m, especially in the southern section (39.5° N).

To corroborate and better figure out surface layer variability, long-term temperature profiles were combined with the SST satellite-based dataset from the CMEMS (Figure 3). For simplicity, Figure 3 presents temperature changes focusing only on the northernmost

(yellow) and southernmost (light blue) selected areas (i.e., P1 and P4), and divided by seasons (considering quarterly slots for each season, i.e., December, January, and February for winter). The SST trend is shown in the upper panels, while temperature anomalies derived from XBT are represented in panels b, c, and d (respectively for the 10–100 m layer, the 100–450 m layer and the 450–800 m layer). Looking at the SST time series in Figure 3a, the annual averages exhibit the typical influence of seasonality, as typically occurs for marginal seas such as the Mediterranean. This results in a substantial temperature difference of nearly 10 °C between winter and summer, hiding significant extreme events and oceanic processes. Even if limited in time, these events have a strong impact on the vertical mixing and transport along the water column. Therefore, a seasonal representation has been adopted to better represent the temporal behaviour of the temperature anomaly in the northern and southern parts of the sub-basin. The surface layer in Figure 3a,b exhibits strong oscillations (and consequently large standard deviations) due to the direct interaction with the atmosphere. Nonetheless, a positive trend is observed in spring, corresponding to the period when the seasonal thermocline is completely eroded, and the surface water layer in the Mediterranean becomes less stratified and more homogenised in depth, with a mean temperature around 13–14 °C. This is also reflected in the low surface standard deviations in winter and spring due to the complex air–sea interaction processes and heat fluxes variability in the Mediterranean Sea [47], with a difference of almost zero between the southern and northern TYS in spring.

Figure 3. SST trend for the North (yellow) and South (cyan) Tyrrhenian Sea (panel (**a**)) vs. temperature anomalies seasonally averaged (panel (**b**–**d**)), with spread represented by the correspondent standard deviations (shaded). (**b**) The 10–100 m layer, (**c**) 100–450 m layer, and (**d**) 450–800 m layer. Red lines in the upper panels highlight the same averaging periods (i.e., 1999–2019).

Looking at deeper layers (i.e., 100–450 m and 450–800 m in Figure 3c,d), a strong increase in the warm anomaly is evident from 2014 to 2018, particularly for the South TYS, after which the positive trend slightly decreases in accordance with Figure 2. Unfortunately, we lack further data beyond March 2019 to verify the robustness of this trend reduction or inversion. However, the SST data suggest a different narrative, as surface observational data indicate significant warming in 2022 and an upward trend.

In general, the temperature anomalies also reflect years with strong winter cooling that produces deep convection, as negative trends are evident in 2005 and 2011–2012, observed from the surface down to 800 m depth. Due to the limited data available, it is not possible to infer positive or negative anomalies for deeper layers (i.e., 800–1500 m), as the values oscillate around zero throughout the years.

To further investigate the subsurface layer, Figure 4 shows the temporal evolution of temperature in the intermediate layer (100–450 m depth) of the TYS, focusing on the northernmost and southernmost points (i.e., P1 and P4). Linear trends and correspondent report tables are shown for the period 2011–2017, respectively, in red and green colours.

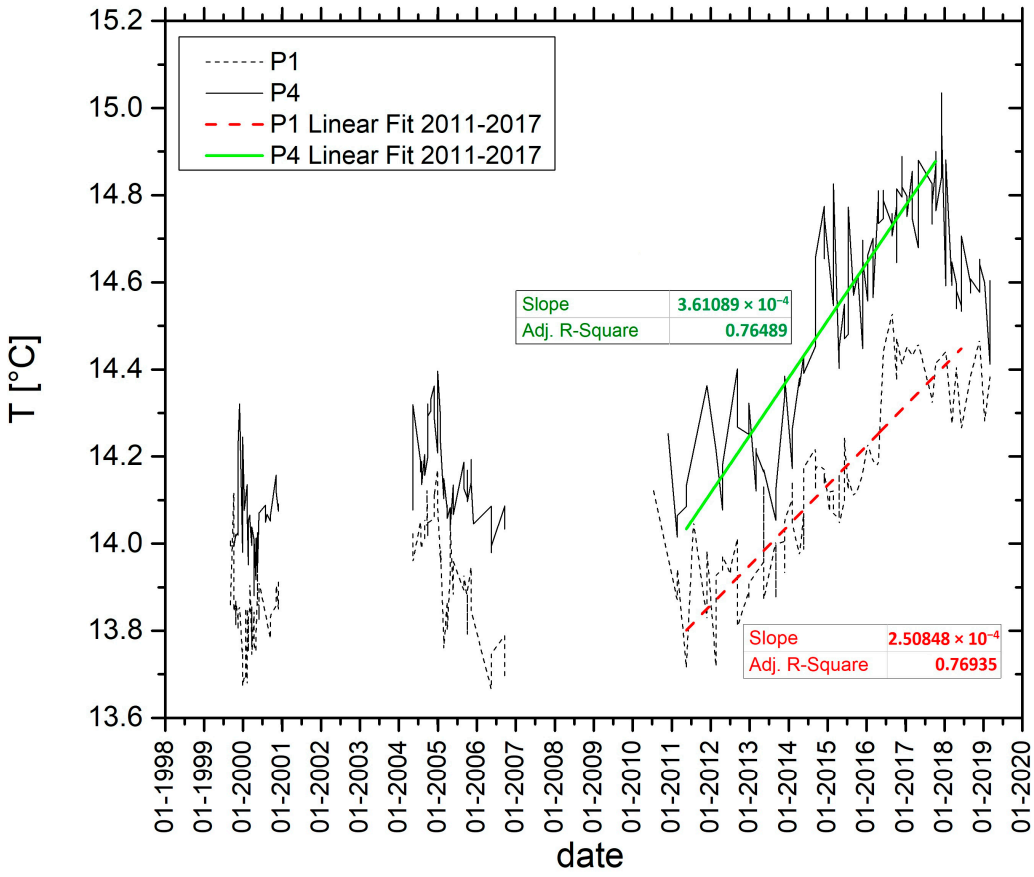

Figure 4. Temporal evolution of mean temperatures for the 100–450 m layer, in the Tyrrhenian Sea at P1 (dotted line) and P4 (continuous black line). Linear trends have been added for the period 2010–2017 for P1 and P4, respectively, in red and green colours, with correspondent report tables in the same colours.

After an initial oscillation period (1999–2000), a positive temperature shift is shown in 2004 to early 2005, followed by a negative trend up to 2006, for both P1 and P4. Since 2014, a sharp increase in temperature has been recorded from north to south. In the southern region (solid line in Figure 4), temperatures rose from 14.1 °C to 14.8 °C between February and December 2014. A similar temperature increase was observed in the northern region, although the highest value (14.5 °C) was reached approximately two years later, in September 2016. This upward trend was interrupted in 2018, when a negative trend was

recorded for both regions. In detail, for P1, the mean temperature changed from 13.87 °C in December 2011 to 14.14 °C in December 2014, reaching 14.40 °C in December 2017, showing an overall increase of 0.53 °C and a slope of 2.51 × 10^{-4}. For P4, the trend was even more marked, with a 0.76 °C increase from 2011 to 2017: the mean temperature rose from 14.12 °C in December 2011 to 14.50 °C in December 2014, and to 14.88 °C in December 2017 with a slope of 3.61 × 10^{-4}. The above computed trends are in agreement with the criterion of significance as their variation over time is greater than 2 × 0.1 °C (i.e., two times their SD in a precautionary estimate, assuming total correlation between temperature measurements). Furthermore, these mean temperature values at P1 are in line with what is shown by [48], where potential temperatures are reported up to the year 2005 at 400 m for the Central TYS. Again, as also shown in Figures 2 and 3, during 2018, there was a drop in mean temperatures. This trend is common to both areas, but more consistent in P4.

Additional information about the water mass evolution over the TYS can be provided through the analysis of the Argo measurements, extracted from the SeaDataNet portal, as detailed in the previous Section 2.2. Figure 5 shows the θ-S diagrams obtained from the available Argo profiles, whose location is shown in the upper maps of the figure. Unfortunately, the data from 2010 to 2013 are missing for the selected areas, and hence two periods have been considered in order to better clarify possible temporal shifts: 2004–2009 (panel a), and 2014–2019 (panel b). Note that surface points with temperatures above 16 °C have been excluded to highlight the intermediate and deep waters. The diagrams are characterised by distinctive hydrological signatures (in agreement with [31,33]), highlighting the presence of LIW with local maxima of temperature and high salinity. Figure 5 confirms the results obtained by XBT profiles, showing a temperature shift toward warmer values for the intermediate waters since 2014, with a minor setback in 2018 (Figure 5b).

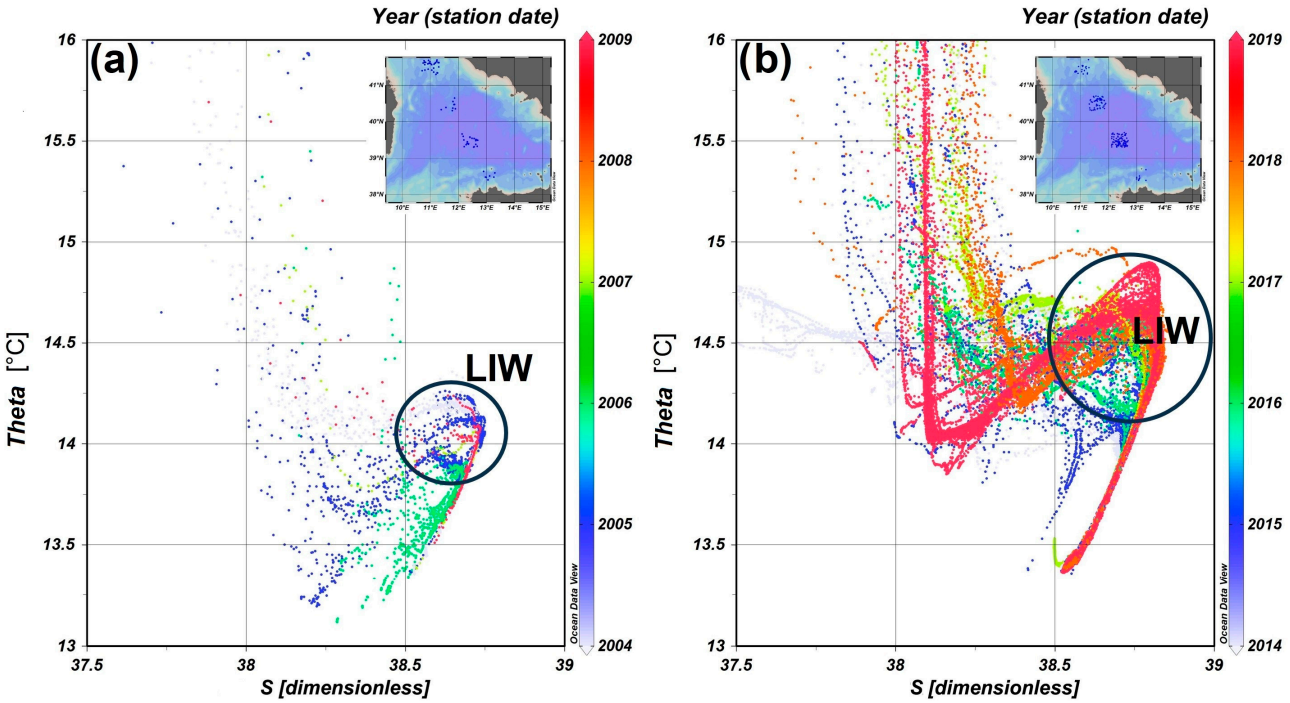

Figure 5. θ-S diagrams from the Argo measurements for the periods 2004–2009 (**a**) and 2014–2019 (**b**). Note that surface temperatures higher than 16 °C have not been included, so as to highlight the intermediate and deep waters.

3.2. OHC Trends and Anomalies

To better figure out TYS dynamics, OHC anomalies were computed in the northern (P1) and southern (P4) sectors of the monitored route. As defined in Section 2.3, anomalies have been defined as the deviation from the baseline period 1999–2019. Figure 6 reports

positive anomalies in red and negative anomalies in blue in three different periods, based on the XBT monitoring activities reported in Table 1: the first period (1999–2001), the second period (2004–2006), and the third period (2010–2019). The three datasets can be considered as reasonably representative of the seasonal condition (i.e., OHC seasonally covered well per each cluster period and depth levels along the route).

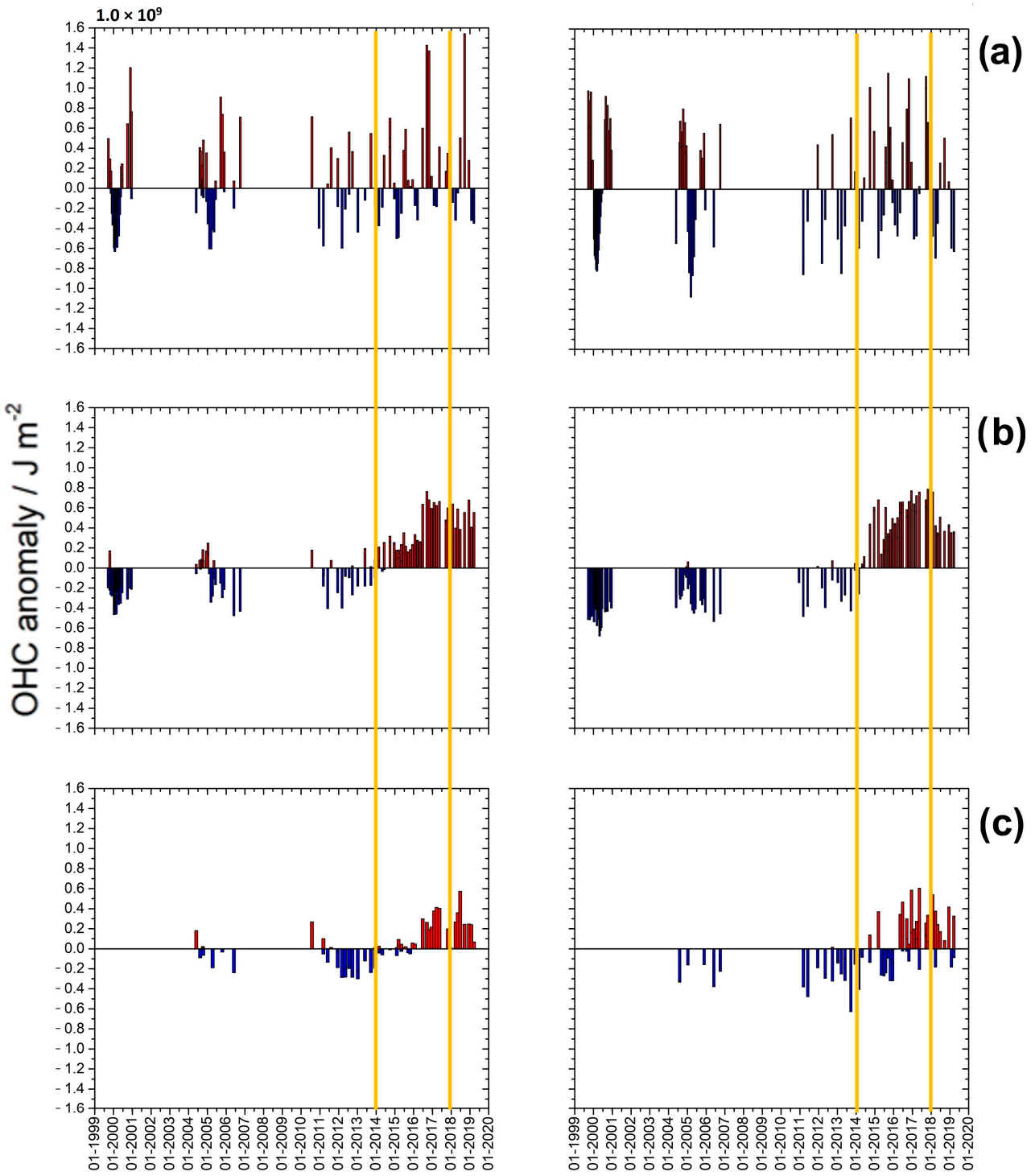

Figure 6. Ocean heat content anomalies computed from XBT data in P1 (left side) and P4 (right side): (**a**) 10–100 m layer; (**b**) 100–450 m layer; (**c**) 450–800 m layer. Black horizontal lines indicate anomalies of 0 J/m^2. Positive anomalies are in red, while negative anomalies are shown in blue. Orange vertical lines are reported for reference to representative years 2014 and 2018.

In the surface levels (10–100 m depth in Figure 6a), OHC anomalies are characterised by strong oscillations around the zero anomaly, in accordance with the SST trend (see Figure 3a), for all three monitoring periods. Again, this is due to the direct interaction with the atmosphere. As regards the subsurface level (100–450 m depth range), a coherent increasing OHC trend is depicted for both areas, especially for the most southward part (i.e., P4), where red positive anomalies are higher, in accordance with the trends shown in Figures 3 and 4. In terms of absolute OHC, mean values along the route are significatively higher in the period 2014–2019 than those of the two previous periods (i.e., 1999–2001 and 2004–2006), for the 100–450 m depth ranges. In particular, after negative levels of OHC anomalies were shown during 2005–2006 and in 2012 and 2013 (shown in blue in Figure 6), the OHC increased, showing positive anomalies (i.e., red bars) and a steeper slope up to 2018 (Figure 6b for both P1 and P4 areas). This positive acceleration is also recorded for the 450–800 m depth ranges but with a 2-year delay (i.e., since 2016, as already pointed out as regards mean temperatures in Figure 4). In general, consistent and continuous positive OHC anomalies (i.e., warming) of the intermediate waters (Figure 6b) appear for the period 2014–2018, and propagate progressively deeper, to the 450–800 m level, in the period 2016–2019, as described by all the anomalies in P1 and by most in P4 (Figure 6c). Again, lower positive anomalies are recorded in 2018, especially considering P4. The maximum OHC anomaly for the 100–450 m layer is $+0.98 \times 10^9$ J/m^2 y^{-1}, recorded in December 2017 in P4. The OHC evolution in the 100–450 m layer (Figure 6b) indicates a steep increase between 2014 and 2017 and a linear trend over the time period 2010–2019 equal to $+0.1 \times 10^9$ J/m^2 y^{-1}, coherently with what is observed in the Sicily Channel [49]. This would lead to the conclusion that the subsurface TYS is warming up more and faster than in the past, in agreement with [49] and [50]. As regards the 450–800 m layer, it is interesting to note that OHC anomalies are constantly almost positive after 2016, with a maximum value of $+0.60 \times 10^9$ J/m^2 y^{-1} in May 2017 for P4 and $+0.57 \times 10^9$ J/m^2 y^{-1} in June 2018 for P1.

Finally, to determine whether this TYS trend is consistent with the rest of the Mediterranean, OHC anomalies derived by XBT measurements have been plotted in Figure 7, together with those derived by the CMEMS data [51]. Larger blue squares indicate the years less covered by XBT data. The XBT trend generally agrees with the OHC anomalies by the CMEMS data from 1999 to 2018 for the whole Mediterranean over the 0–700 m water layer.

Also, a negative trend is evident in 2005 and 2011–2012 (as pointed out by [28] and in accordance with Figures 4 and 6), while from 2014 the TYS started warming quickly (again in agreement with our Figures 4 and 6 and with [9,41]). From this figure, it is possible to infer three different clusters (referred as A, B, and C in the plot): Cluster A (corresponding to the years 2004, 2005, and 2006), when Tyrrhenian anomalies are in phase with those of the Mediterranean Sea; Cluster B (i.e., from 2010 to 2013), when Tyrrhenian anomalies show a different trend with respect to the Mediterranean whole basin, especially for 2011 and 2013 when strong dense water formation events in the western Mediterranean take place [12,28,52]; and Cluster C (i.e., from 2014 to 2018), characterised by general fast warming, shows a different trend with respect to the Mediterranean whole basin, especially for 2015 and 2017 (opposite warming up) and 2018 (opposite negative trend).

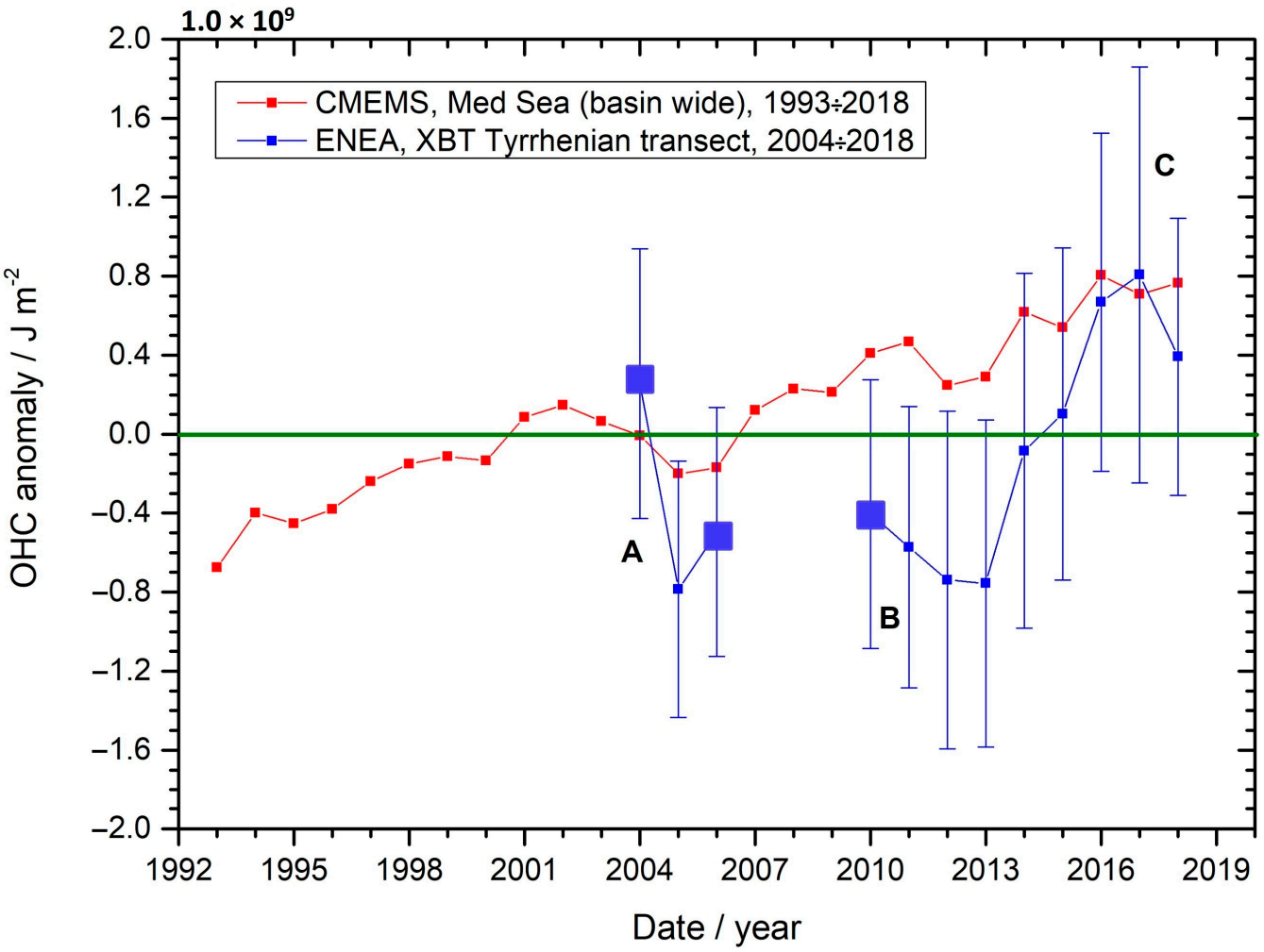

Figure 7. Time series of annual mean area averaged ocean heat content in the Mediterranean Sea (basin-wide) integrated over the 0–700 m depth layer during 1993–2018 (from [51]), plotted against time series of annual mean area averaged ocean heat content in the Tyrrhenian Sea obtained from XBT data discussed in the present paper (± standard deviation shown as error bars in blue). Three different clusters (referred to as A, B, and C in the plot) can be inferred, as detailed in the main text. Larger blue square points indicate the years less covered by XBT data, while the green line indicate the reference for zero anomaly.

3.3. Deep-Water Exchanges through the Sardinia Channel

Despite the lack of extensive data for the deep TYS, it is evident that this large heat reservoir may have unpredictable future impacts on the physical and biological oceanographic mechanisms throughout the western Mediterranean basin, considering specifically the deep water TYS outflow through the Sardinia channel, up to 2000 m [18,53]. To monitor and better understand the impact that the TYS heat reservoir can induce, the deep-water mass exchanges between the TYS and the western sub-basin were taken into account. Specifically, the inflow and outflow through the Sardinia Channel were examined using reanalysis data, drawing on the work of [30], which already explored the impact of TYS deep water on the Mediterranean's western circulation. The idea is to consider the transport along this channel as a fingerprint of the variability and trend of the TYS circulation and its internal dynamics. Following the clusters identified in Figure 7, annual averages of the current model component U were extracted from CMEMS (Figure 8) at three points across the Sardinia Channel (M1, M2, and M3 in Figure 8d). This approach aims to reveal potential variations in the TYS outflow regime across the different climatic phases identified in Section 3.2. Figure 8 illustrates the vertical structure of the flow across the Channel, with

positive values indicating an eastward annual averaged component of the current velocity. The outflow regime is shown in M1 and M3, located at the channel's edge corners, consistent with descriptions in [30] (Figure 5) and [53] (Figure 1c), as well as other references. The inflow regime dominates the central part of the channel (i.e., M2), as confirmed by several in situ observations and modelling experiments [26,53]. In general, a fair amount of interannual variability can be observed in all profiles. In addition, an analysis of all clusters reveals that profiles from the period of greater warming (cluster C reported in Figure 8c) exhibit the most variability, especially in M2, where a regime shift is observed during the warmest years.

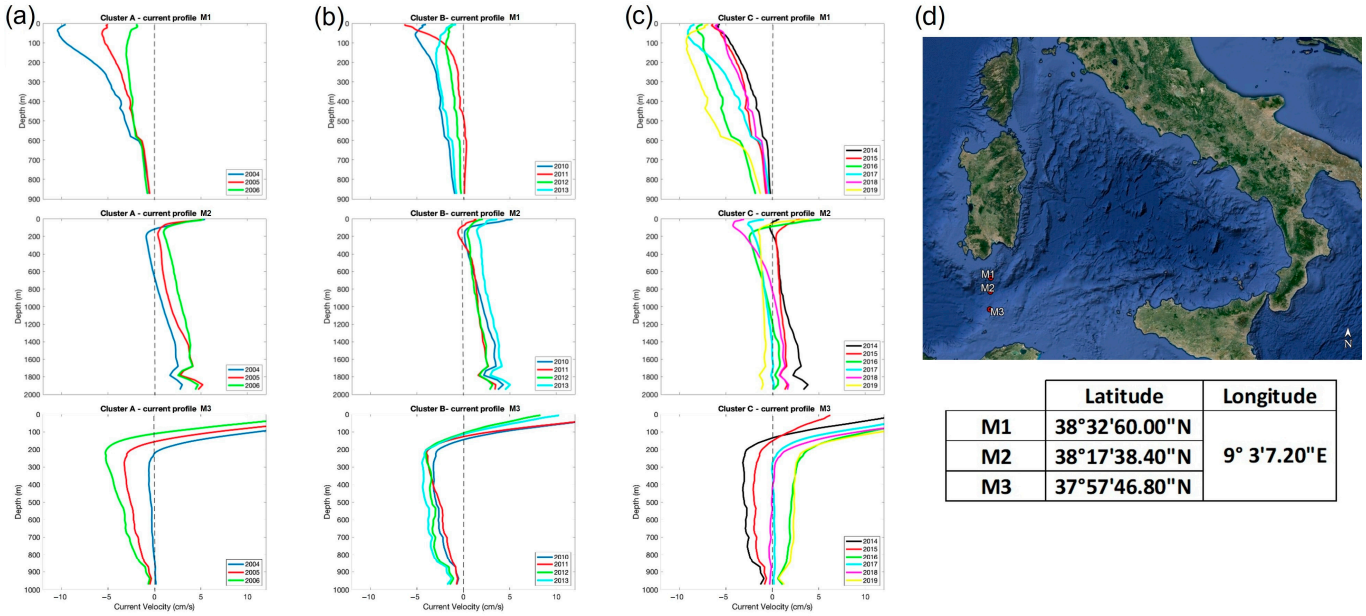

	Latitude	Longitude
M1	38°32'60.00"N	9° 3'7.20"E
M2	38°17'38.40"N	
M3	37°57'46.80"N	

Figure 8. Profiles of the current component U (panel (**a**–**c**)) for three points of the Sardinia Channel (panel (**d**)) extracted from CMEMS [51] for different years. Positive values indicate an eastward annual averaged component of the current velocity (cm/s). Different colours indicate different years. Panels follow the division into clusters made in Figure 7: (**a**) is correspondent to the years from 2004 to 2006; (**b**) from 2010 to 2013; and (**c**) from 2014 to 2019.

4. Discussion

The integrated approach used for analysing data along different sections revealed interesting structures and variabilities. Figure 2 shows, during winter, periodic intermediate-deep convective events affecting layers from 0 to 200 m, mainly in the northern part of the basin, in agreement with what [54] observed in the northwestern Mediterranean Sea.

As regards intermediate layers (100–450 m), the XBT data align with the findings of [48], which reports a progressive heat and salt accumulation at intermediate levels in the Ligurian and Tyrrhenian Sea, with the highest salt and heat contents recorded in 2003–2004 (see also their Figure 4b). This increase depicted the signal of the propagation of a climatic transient, commonly known as the Eastern Mediterranean Transient (EMT, [55,56]), which is also evident in the TYS, as shown by our Figures 4 and 5 for temperature. The intense deep water formation process occurred in the Gulf of Lion in 2004–2005, bringing a significant amount of salt and heat towards the deep layer, as evidenced by the reduction in salt and heat content in the LIW during the succeeding months (Figure 5b of [48] and light green points in our Figure 5a). Similarly, XBT data in Figures 4 and 6 show a negative inflection in temperature and OHC anomalies during winter 2005, originating in the southern TYS and then propagating in the northern TYS.

Later on, the analysed datasets consistently revealed the same pattern across both the temporal and spatial dimensions (including geographical and depth directions). Coherently

with the recent literature [10,12,13], abrupt warming was recorded in all TYS zones around 2014 (Figures 2–7). As a result of the global atmospheric warming, subsurface water masses become progressively warmer, stratifying stably enough to create a kind of cap that hinders deep convection and in turn mixing with the rest of the water column. This is consistent with the entry of a warmer LIW southward that contributes to increasing the heat content in the intermediate layers (Figure 5), exacerbating the warming signal up to 800 m depth. This warming signal then spreads northwards due to the gyre's circulation and advection, increasing turbulence due to the influence of quasi-permanent cyclonic/anticyclonic circulation activity (e.g., the Bonifacio double gyre circulation), as well as topographic features that promote continuous mixing.

The temperatures and OHC shown in Figures 3–6 also reflect the increase in warming around 2014. In Figure 3b–d): from 100 to 800 m depth, there is a shift from a thermodynamic equilibrium to another with a higher equilibrium state. The year 2014 appears to be the period when the massive warming of the TYS took on large coherent spatial and temporal features, as also confirmed by Argo measurements (Figure 5b). During this period, the entire system warmed, progressively accumulating more thermal energy. Moreover, during this period, the SST trends show a continuous and quite homogeneous warming both in the northern and in the southern parts of the Tyrrhenian Basin (Figure 3a). The anomalous warming of the LIW in the TYS was also documented by [41,57], with a peak of this anomaly around 2014 [28]. In particular, the latter study suggests that the lack of intense deep convective winters between 2014 and 2018 resulted in a strong stratification. This allowed the LIW, with its high temperature and salinity contents, to "invade" the TYS, spreading up to the Ligurian Basin while preserving its core.

The present results go further, showing a new scenario also in the TYS thermohaline circulation. The whole TYS basin undergoes a sort of positive feedback: the ongoing warming increases the stability of its stratification, and it acts as a significant heat reservoir affecting the western Mediterranean thermohaline circulation that in turn exacerbates the TYS hydrological equilibrium, typical of warming oceans. This is in line with refined analyses of available worldwide observations, showing an increase in global stratification that is twice that estimated from 1970 to 2018 [58].

More likely, it is due to a non-linear combination between two synergistic processes: firstly, a well-known climate trend leading to local surface warming resulting from atmosphere interaction (noted for the whole Mediterranean Sea), and secondly, local subsurface warming resulting from the advection of warm water masses originating from the Levantine Basin. As a fact, the positive feedback particularly affects the intermediate southern layer, which initially experienced the arrival of a warmer and saltier LIW (Figures 4 and 6b) in accordance with [33]. A "blob" of warm water around 100–450 m passed the Sicily Channel, and mixed and transferred its heat to the entire water column, impacting TYS water mass transformation and deep water. Subsequently, the warming signal propagated northward, producing an extraordinary hydrological change in the central part of the TYS basin that affected deeper layers down to 1000–1500 m (Figure 2).

Furthermore, looking at Figure 8, it is possible to infer that in addition to the well-known surface and intermediate heat transfer occurring through the Corsican Channel and influencing the precondition for the dense water formation in the northwestern Mediterranean, an additional heat injection can come through the Sardinian Channel (maximum depth of about 2000 m). This further heat can ultimately impact the processes responsible for producing cold, dense, and oxygenated water in the deepest layers which then return to the TYS, generating a positive feedback loop that exacerbates the warming trend. Differences between the general Mediterranean and the TYS trends shown in Figure 6 could be explained by the influence of the North Ionian Gyre on the redistribution of intermediate waters ([59–63]). Regarding the intermediate layer, the time series presented in this study align with comparable time series collected in the Sicily Channel (see, for example, Figure 6 of [64] or [65]). These series highlight a general increasing trend and the presence of "cyclic patterns" in temperature and salinity, which could be associated with

the alternation between different circulation modes (cyclonic and anticyclonic) of the North Ionian Gyre, in addition to the above-mentioned intermediate water formation processes.

Given its central location within the Mediterranean and its interactions with neighbouring sub-basins, the results of these analyses suggest that the TYS acts as a magnifying glass for the whole OHC variability of the Mediterranean Sea. It reveals local details of a significantly increased warming trend over the past few decades [1,9,55] whose impacts are expected to become more apparent in the coming decades. The data used also allowed us to distinguish between heat sources: direct intake from the surface, which is largely influenced by seasonal variability, and an interior signal (at about 100 m depth) resulting from the advection of water masses originating elsewhere in the Mediterranean, such as the LIW, carrying a climatic signal. Figures 3a and 6a show indeed that no acceleration with a distinct pattern from deeper levels can be observed from SST and surface OHC anomalies.

5. Conclusions and Perspectives

The present paper, through the use of a relevant number of XBT observations (almost 2000) along the SOOP Genoa–Palermo route, has proven how the TYS sub-basin is an ideal site for the detection of variability, trends, and long-term changes in climate variables (e.g., the temperature anomaly and OHC), as well as for the assessment of the related impacts at regional and local scales. The overall XBT accuracy stated by the manufacturer is 0.2 °C [66,67] and, as described by [36,37], many phenomena can contribute to the uncertainties in measurements made by XBTs, and they can act either on the depth or on the temperature, or on both. Ref. [37] verified that the calculated depth for the XBT overestimates the actual depth in the first tens of metres of the fall. Considering that for any depth value up to 250 m, the associated uncertainty is 5 m and do not infer in the general baseline computation for anomaly and OHC as this was derived from a uniform dataset of only XBTs, no corrections have been applied to the XBT depth values in this paper. Recent results [37] on the intercomparison of XBT data, Argo, and ship-based CTD profiles in the Mediterranean Sea, confirmed the metrological robustness of XBT data, proving the reliability of the 20-year XBT dataset here reported and the related analyses. Even if the obtained results could certainly be improved in terms of temperature mean difference and standard deviation, considering its spatial and temporal coverage, the used XBT long-term dataset has been very effective in studying thermal anomalies, capturing a general warming trend across the TYS sub-basin, as well as the deepening of the heat signal in underlying layers. A large spatial (north–south) variability of the TYS thermal characteristics along the SOOP Genoa–Palermo route (Figure 1) has been recorded at all monitored depths (10–1500 m) (Figure 2).

Our results have underlined how the role of circulation is essential to this variability: based on the literature [18,24,28], it seems linked to non-linear interactions among several driving forces such as the advection of water masses from western and eastern Mediterranean Sea and wind stress. These generate large gyre/eddy variability in time and space that results in quasi-permanent structures in the northern part of the TYS [15] and much less permanent and coherent gyres/eddies in its southern part [31]. The variability of the gyre/eddy has an impact on the upwelling/downwelling intensity and therefore on the distribution of the surface/subsurface warming signal into the deep and abyssal layers.

Furthermore, our analysis has shown that periodically, temperature trends detected in the TYS might differ from those of the Mediterranean as a whole. This is probably due to the Tyrrhenian's response to the decadal oscillation of the North Ionian Gyre, which, acting as a "manifold" between the eastern and western basins, influences the redistribution of Levantine Intermediate Water (LIW) towards the western Mediterranean at the intermediate level, highlighting important remote forcing, while the surface is related to interannual variability, and is mainly wind-driven. In this prospective, the Sardinia Channel is a crucial passage to monitor in order to follow not only the water mass inflow in the TYS, but also to assess the possible impact of TYS deep water in the deep convection

processes of the western Mediterranean and their efficiency in supporting vital processes such as thermohaline circulation and abyssal ventilation [68].

An additional key element is then played by the TYS bathymetry: its typical V-shape morphology reaching depths of up to 4000 m greatly influences both circulations and physical processes [18], making the TYS an active heat reservoir, and by consequence a hotspot in the hotspot. The peculiar morphology of the TYS prompts us to adopt a zonal subdivision of the dataset into four different areas that well represent the local/regional climate variability with respect to the general behaviour recorded for the Mediterranean Sea [1].

More generally, the present work should act as a stimulus to identify further observational and modelling methodologies tailored to better study the complexity of the impact of climate change in the TYS, the TYS itself being a sort of nested hotspot representative of the climate change context of the Western Mediterranean. Considering the shift recorded also for the deepest levels, observation campaigns and fixed stations should be developed to collect more deep-sea data to monitor the physical heat uptake mechanism along the whole water column.

Author Contributions: Conceptualization, T.C., N.L.B. and V.A.; methodology, T.C., N.L.B. and V.A.; software, T.C., G.R. and S.M.; data processing and analysis, T.C., G.R., N.L.B. and S.M.; writing—original draft preparation, T.C.; writing—review and editing, T.C., N.L.B. and V.A.; funding acquisition, T.C. and G.R. All authors have read and agreed to the published version of the manuscript.

Funding: This work was supported and funded by Agenzia nazionale per le nuove tecnologie, l'energia e lo sviluppo economico sostenibile (ENEA).

Institutional Review Board Statement: Not applicable.

Informed Consent Statement: Not applicable.

Data Availability Statement: The full XBT datasets used for this analysis can be downloaded from the Pan-European infrastructure for ocean and marine data management at https://cdi.seadatanet.org (European Commission, 2007, accessed on 30 July 2024) and/or from the World Ocean Database at https://www.ncei.noaa.gov/products/world-ocean-database (WOD, 2018 accessed on 30 July 2024). Bathymetry along the XBT track used values from the European Marine Observation and Data Network (see http://portal.emodnet-bathymetry.eu/mean-depth-full-coverage, accessed on 30 July 2024). Current data are available from the Copernicus Marine Environment Monitoring Service (CMEMS) at the following link: https://doi.org/10.25423/CMCC/MEDSEA_MULTIYEAR_PHY_006_004_E3R1 (accessed on 30 July 2024). The Mediterranean Sea Surface Temperature dataset used in this paper is freely distributed through CMEMS (http://marine.copernicus.eu, accessed on 30 July 2024) and identified as SST_MED_SST_L4_REP_OBSERVATIONS_010_021 in the CMEMS catalogue (https://doi.org/10.48670/moi-00173, accessed on 30 July 2024). This study has also been conducted using Copernicus Marine Service Information (https://marine.copernicus.eu/) for the Mediterranean OHC estimate.

Acknowledgments: Part of the XBT probes deployed in the period 2011–2013 were kindly provided by AOML/NOAA in the framework of JCOMM/SOOP activities. Many thanks to the shipping company Grandi Navi Veloci (owner of the ships used for the monitoring on the Genoa–Palermo transect) for their decades-long collaboration since September 1999, and to Hapag Lloyd and CMA CGM for the period December 2007–March 2011. The authors acknowledge F. Reseghetti for the extensive monitoring activity with XBT probes, and for many suggestions and discussions.

Conflicts of Interest: The authors declare no conflicts of interest.

References

1. Pisano, A.; Marullo, S.; Artale, V.; Falcini, F.; Yang, C.; Leonelli, F.E.; Santoleri, R.; Nardelli, B.B. New Evidence of Mediterranean Climate Change and Variability from Sea Surface Temperature Observations. *Remote Sens.* **2020**, *12*, 132. [CrossRef]
2. Lionello, P.; Scarascia, L. The relation between climate change in the Mediterranean region and global warming. *Reg. Environ. Chang.* **2018**, *18*, 1481–1493. [CrossRef]

3. Vargas-Yáñez, M.; Zunino, P.; Benali, A.; Delpy, M.; Pastre, F.; Moya, F.; García-Martínez, M.d.C.; Tel, E. How much is the western Mediterranean really warming and salting? *J. Geophys. Res.* **2010**, *115*, C04001. [CrossRef]
4. Bindoff, N.L.; Willebrand, J.; Artale, V.; Cazenave, A.; Gregory, J.M.; Gulev, S.; Hanawa, K.; Le Quere, C.; Levitus, S. Observations: Oceanic Climate Change and Sea Level. In *Climate Change 2007: The Physical Science Basis. Contribution of Working Group I to the Fourth Assessment Report of the Intergovernmental Panel on Climate Change*; Solomon, S., Qin, D., Manning, M., Chen, Z., Marquis, M., Averyt, K.B., Tignor, M., Miller, H.L., Eds.; Cambridge University Press: Cambridge, UK; New York, NY, USA, 2007.
5. Seager, R.; Osborn, T.J.; Kushnir, Y.; Simpson, I.R.; Nakamura, J.; Liu, H. Climate Variability and Change of Mediterranean-Type Climates. *J. Clim.* **2019**, *32*, 2887–2915. [CrossRef]
6. MedECC. Climate and Environmental Change in the Mediterranean Basin—Current Situation and Risks for the Future. In *First Mediterranean Assessment Report*; Cramer, W., Guiot, J., Marini, K., Eds.; Union for the Mediterranean, Plan Bleu, UNEP/MAP: Marseille, France, 2020; ISBN 978-2-9577416-0-1. [CrossRef]
7. Pastor, F.; Valiente, J.; Palau, J. Sea surface temperature in the Mediterranean: Trends and spatial patterns (1982–2016). *Pure Appl. Geophys.* **2018**, *11*, 4017–4029. [CrossRef]
8. Shaltout, M.; Omstedt, A. Recent Sea surface temperature trends and future scenarios for the Mediterranean Sea. *Oceanologia* **2014**, *56*, 411–443. [CrossRef]
9. Cheng, L.; Abraham, J.; Trenberth, K.E.; Fasullo, J.; Boyer, T.; Mann, M.E.; Zhu, J.; Wang, F.; Locarnini, R.; Li, Y.; et al. Another Year of Record Heat for the Oceans. *Adv. Atmos. Sci.* **2023**, *40*, 963–974. [CrossRef]
10. Cheng, L.; Abraham, J.; Trenberth, K.E.; Fasullo, J.; Boyer, T.; Locarnini, R.; Zhang, B.; Yu, F.; Wan, L.; Chen, X.; et al. Upper Ocean Temperatures Hit Record High in 2020. *Adv. Atmos. Sci.* **2021**, *38*, 523–530. [CrossRef]
11. Krauzig, N.; Falco, P.; Zambianchi, E. Contrasting surface warming of a marginal basin due to large-scale climatic patterns and local forcing. *Nat. Sci. Rep.* **2020**, *10*, 17648. [CrossRef]
12. von Schuckmann, K.; Le Traon, P.-Y.; Smith, N.; Pascual, A.; Djavidnia, S.; Gattuso, J.-P.; Grégoire, M.; Nolan, G.; Aaboe, S.; Fanjul, E.; et al. Copernicus Marine Service Ocean State Report, Issue 4. *J. Oper. Oceanogr.* **2020**, *13*, s1–s172. [CrossRef]
13. Storto, A.; Masina, S.; Simoncelli, S.; Iovino, D.; Cipollone, A.; Drevillon, M.; Drillet, Y.; von Schuckman, K.; Parent, L.; Garric, G.; et al. The added value of the multi-system spread information for ocean heat content and steric sea level investigations in the CMEMS GREP ensemble reanalysis product. *Clim. Dyn.* **2019**, *53*, 287–312. [CrossRef]
14. Malanotte-Rizzoli, P.; Artale, V.; Borzelli-Eusebi, G.L.; Brenner, S.; Crise, A.; Gacic, M.; Kress, N.; Marullo, S.; D'ALcalà, M.R.; Sofianos, S.; et al. Physical forcing and physical/biochemical variability of the Mediterranean Sea: A review of unresolved issues and directions for future research. *Ocean Sci.* **2014**, *10*, 281–322. [CrossRef]
15. Ciuffardi, T.; Napolitano, E.; Iacono, R.; Reseghetti, F.; Raiteri, G.; Bordone, A. Analysis of surface circulation structures along a frequently repeated XBT transect crossing the Ligurian and Tyrrhenian Seas. *Ocean Dyn.* **2016**, *66*, 767–783. [CrossRef]
16. Krivosheya, V.G. Water circulation and structure in the Tyrrhenian Sea. *Oceanology* **1983**, *23*, 166–171.
17. Millot, C. Circulation in the Western Mediterranean Sea. *J. Mar. Syst.* **1999**, *20*, 423–442. [CrossRef]
18. Vetrano, A.; Napolitano, E.; Iacono, R.; Schroeder, K.; Gasparini, G.P. Tyrrhenian Sea circulation and water mass fluxes in spring 2004: Observations and model results. *J. Geophys. Res.* **2010**, *115*, C06023. [CrossRef]
19. Durante, S.; Schroeder, K.; Mazzei, L.; Pierini, S.; Borghini, M.; Sparnocchia, S. Permanent thermohaline staircases in the Tyrrhenian Sea. *Geophys. Res. Lett.* **2019**, *46*, 1562–1570. [CrossRef]
20. de la Vara, A.; Parras-Berrocal, I.M.; Izquierdo, A.; Sein, D.V.; Cabos, W. Climate change signal in the ocean circulation of the Tyrrhenian Sea. *Earth Syst. Dynam.* **2022**, *13*, 303–319. [CrossRef]
21. von Schuckmann, K.; Le Traon, P.Y.; Smith, N.; Pascual, A.; Djavidnia, S.; Brasseur, P.; Grégoire, M. Copernicus Ocean State Report, Issue 6. *J. Oper. Oceanogr.* **2022**, *15*, s1–s220. [CrossRef]
22. Marullo, S.; Serva, F.; Iacono, R.; Napolitano, E.; di Sarra, A.; Meloni, D.; Monteleone, F.; Sferlazzo, D.; De Silvestri, L.; de Toma, V.; et al. Record-breaking persistence of the 2022/23 marine heatwave in the Mediterranean Sea. *Environ. Res. Lett.* **2023**, *18*, 114041. [CrossRef]
23. Gille, S.T.; Metzger, E.J.; Tokmakian, R. Seafloor Topography and Ocean Circulation. *Oceanography* **2004**, *17*, 47–54. [CrossRef]
24. Artale, V.; Astraldi, M.; Buffoni, G.; Gasparini, G.P. Seasonal variability of gyre-scale circulation in the northern Tyrrhenian Sea. *J. Geophys. Res.* **1994**, *99*, 14127–14137. [CrossRef]
25. Astraldi, M.; Gasparini, G.P. The seasonal characteristics of the circulation in the Tyrrhenian Sea. In *Seasonal and Interannual Variability of the Western Mediterranean Sea*; Coastal and Estuarine Studies; Geophysical Monograph Series; La Violette, P., Ed.; American Geophysical Union: Washington, DC, USA, 1994; Volume 46, pp. 115–134. [CrossRef]
26. Astraldi, M.; Gasparini, G.P.; Vetrano, A.; Vignudelli, S. Hydrographic characteristics and interannual variability of water masses in the central Mediterranean: A sensitivity test for long-term changes in the Mediterranean Sea. *Deep Sea Res.* **2002**, *49*, 661–680. [CrossRef]
27. Hopkins, T.S. Recent observations on the intermediate and deep water circulation in the southern Tyrrhenian Sea. *Oceanol. Acta* **1988**, *9*, 41–50.
28. Schroeder, K.; Chiggiato, J.; Bryden, H.L.; Borghini, M.; Ben Ismail, S. Abrupt climate shift in the Western Mediterranean Sea. *Sci. Rep.* **2016**, *6*, 23009. [CrossRef]
29. Sparnocchia, S.; Gasparini, G.P.; Astraldi, M.; Borghini, M.; Pistek, P. Dynamics and mixing of the Eastern Mediterranean outflow in the Tyrrhenian basin. *J. Mar. Syst.* **1999**, *20*, 301–317. [CrossRef]

30. Rhein, M.; Send, U.; Klein, B.; Krahmann, G. Interbasin deep water exchange in the western Mediterranean. *J. Geophys. Res.* **1999**, *104*, 23495–23508. [CrossRef]
31. Iacono, R.; Napolitano, E.; Palma, M.; Sannino, G. The Tyrrhenian Sea Circulation: A Review of Recent Work. *Sustainability* **2021**, *13*, 6371. [CrossRef]
32. Millot, C.; Taupier-Letage, I. Circulation in the Mediterranean Sea. In *The Handbook of Environmental Chemistry: Water Pollution*; Saliot, A., Ed.; Springer: Berlin/Heidelberg, Germany, 2005; Volume 5, pp. 29–66. [CrossRef]
33. Napolitano, E.; Iacono, R.; Ciuffardi, T.; Reseghetti, F.; Poulain, P.M.; Notarstefano, G. The Tyrrhenian Intermediate Water (TIW): Characterization and formation mechanisms. *Prog. Oceanogr.* **2019**, *170*, 53–68. [CrossRef]
34. Simoncelli, S.; Reseghetti, F.; Fratianni, C.; Cheng, L.; Raiteri, G. Reprocessing of XBT profiles from the Ligurian and Tyrrhenian seas over the time period 1999–2019 with full metadata upgrade. *Earth Syst. Sci. Data Discuss.* **2024**. *preprint*. [CrossRef]
35. Ciani, D.; Rio, M.H.; Menna, M.; Santoleri, R. A synergetic approach for the space-based sea surface currents retrieval in the Mediterranean Sea. *Remote Sens.* **2019**, *11*, 1285. [CrossRef]
36. Reseghetti, F.; Cheng, L.; Borghini, M.; Yashayaev, I.M.; Raiteri, G.; Zhu, J. Assessment of Quality and Reliability of Measurements with XBT Sippican T5 and T5/20. *J. Atmos. Ocean. Technol.* **2018**, *35*, 1935–1960. [CrossRef]
37. Bordone, A.; Pennecchi, F.; Raiteri, G.; Repetti, L.; Reseghetti, F. XBT, ARGO Float and Ship-Based CTD Profiles Intercompared under Strict Space-Time Conditions in the Mediterranean Sea: Assessment of Metrological Comparability. *J. Mar. Sci. Eng.* **2020**, *8*, 313. [CrossRef]
38. Gille, S.T. Float observations of the Southern Ocean: Part 1, Estimating mean fields, bottom velocities, and topographic steering. *J. Phys. Oceanogr.* **2003**, *33*, 1167–1181. [CrossRef]
39. Marshall, D. Influence of Topography on the Large-Scale Ocean Circulation. *J. Phys. Oceanogr.* **1995**, *25*, 1622–1635. [CrossRef]
40. Pinardi, N.; Masetti, E. Variability of the large-scale general circulation of the Mediterranean Sea from observations and modelling: A review. Palaeogeography, Palaeoclimatology. *Palaeoecology* **2000**, *158*, 153–173. [CrossRef]
41. Ribotti, A.; Sorgente, R.; Olita, A.; Orilia, F.; Borghini, M.; Reseghetti, F. Indication of recent warming process at the intermediate level in the Tyrrhenian Sea from SOOP XBT measurements. *Mediterr. Mar. Sci.* **2016**, *17*, 467–475. [CrossRef]
42. von Schuckmann, K.; Le Traon, P.-Y.; Smith, N.; Pascual, A.; Brasseur, P.; Fennel, K.; Djavidnia, S.; Aaboe, S.; Fanjul, E.A.; Autret, E.; et al. Ocean heat content. The Copernicus Marine Environment Monitoring Service Ocean State Report, issue 2. *J. Oper. Oceanogr.* **2018**, *11*, s1–s142. [CrossRef]
43. Palmer, M.D.; Roberts, C.D.; Balmaseda, M.; Chang, Y.-S.; Chepurin, G.; Ferry, N.; Fujii, Y.; Good, S.A.; Guinehut, S.; Haines, K.; et al. Ocean heat content variability and change in an ensemble of ocean reanalyses. *Clim. Dyn.* **2017**, *49*, 909–930. [CrossRef]
44. Liu, W.; Xie, S.P.; Lu, J. Tracking Ocean heat uptake during the surface warming hiatus. *Nat. Commun.* **2016**, *7*, 10926. [CrossRef]
45. von Schuckmann, K.; Gaillard, F.; Le Traon, P.Y. Global hydrographic variability patterns during 2003–2008. *J. Geophys. Res.* **2009**, *114*, C09007. [CrossRef]
46. Schlitzer, R. Ocean Data View 2021. Available online: https://odv.awi.de (accessed on 30 July 2024).
47. Jordà, G.; Von Schuckmann, K.; Josey, S.; Caniaux, G.; García-Lafuente, J.; Sammartino, S.; Özsoy, E.; Polcher, J.; Notarstefano, G.; Poulain, P.-M.; et al. The Mediterranean Sea Heat and Mass Budgets: Estimates, Uncertainties and Perspectives. *Prog. Oceanogr.* **2017**, *156*, 174–208. [CrossRef]
48. Schroeder, K.; Gasparini, G.P.; Tangherlini, M.; Astraldi, M. Deep and intermediate water in the western Mediterranean under the influence of the Eastern Mediterranean Transient. *Geophys. Res. Lett.* **2006**, *33*, 21. [CrossRef]
49. Cheng, L.; Abraham, J.; Trenberth, K.E.; Fasullo, J.; Boyer, T.; Mann, M.E.; Zhu, J.; Wang, F.; Locarnini, R.; Li, Y.; et al. Another Record: Ocean Warming Continues through 2021 despite La Niña Conditions. *Adv. Atmos. Sci.* **2022**, *39*, 373–385. [CrossRef] [PubMed]
50. Ben Ismail, S.; Schroeder, K.; Chiggiato, J.; Sparnocchia, S.; Borghini, M. *Long Term Changes Monitored in Two Mediterranean Channels. Copernicus Marine Service Ocean State Report 2021, Issue 5*; von Schuckmann, K., Le Traon, P.-Y., Eds.; Informa UK Limited, trading as Taylor & Francis Group: Milton Park, UK, 2021; pp. 48–52. [CrossRef]
51. Escudier, R.; Clementi, E.; Cipollone, A.; Pistoia, J.; Drudi, M.; Grandi, A.; Lyubartsev, V.; Lecci, R.; Aydogdu, A.; Delrosso, D.; et al. A High Resolution Reanalysis for the Mediterranean Sea. *Front. Earth Sci.* **2021**, *9*, 1060. [CrossRef]
52. Margirier, F.; Testor, P.; Heslop, E.; Mallil, K.; Bosse, A.; Houpert, L.; Mortier, L.; Bouin, M.-N.; Coppola, L.; D'Ortenzio, F.; et al. Abrupt warming and salinification of intermediate waters interplays with decline of deep convection in the Northwestern Mediterranean Sea. *Sci. Rep.* **2020**, *10*, 20923. [CrossRef]
53. Vetrano, A.; Gasparini, G.P.; Molcard, R.; Astraldi, M. Water flux estimates in the central Mediterranean Sea from an inverse box model. *J. Geophys. Res.* **2004**, *109*, C01019. [CrossRef]
54. Schroeder, K.; Josey, S.A.; Herrmann, M.; Grignon, L.; Gasparini, G.P.; Bryden, H.L. Abrupt warming and salting of the Western Mediterranean Deep Water after 2005: Atmospheric forcings and lateral advection. *J. Geophys. Res.* **2010**, *115*, C08029. [CrossRef]
55. Roether, W.; Manca, B.B.; Klein, B.; Bregant, D.; Georgopoulos, D.; Beitzel, V.; Kovačević, V.; Luchetta, A. Recent Changes in Eastern Mediterranean Deep Waters. *Science* **1996**, *271*, 333–335. [CrossRef]
56. Tanhua, T.; Hainbucher, D.; Schroeder, K.; Cardin, V.; Alvarez, M.; Civitarese, G. The Mediterranean Sea system: A review and an introduction to the special issue. *Ocean. Sci.* **2013**, *9*, 789–803. [CrossRef]
57. Smith, R.O.; Bryden, H.L.; Stansfield, K. Observations of new western Mediterranean deep water formation using Argo floats 2004–2006. *Ocean Sci.* **2008**, *4*, 133–149. [CrossRef]

58. IPCC. *Climate Change 2021: The Physical Science Basis. Contribution of Working Group I to the Sixth Assessment Report of the Intergovernmental Panel on Climate Change*; Masson-Delmotte, V., Zhai, P., Pirani, A., Connors, S.L., Péan, C., Berger, S., Caud, N., Chen, Y., Goldfarb, L., Gomis, M.I., et al., Eds.; Cambridge University Press: Cambridge, UK; New York, NY, USA, 2021; p. 2391. [CrossRef]
59. Borzelli, G.L.E.; Gačić, M.; Cardin, V.; Civitarese, G. Eastern Mediterranean Transient and Reversal of the Ionian Sea Circulation. *Geophys. Res. Lett.* **2009**, *36*, L15108. [CrossRef]
60. Gačić, M.; Borzelli, G.L.E.; Civitarese, G.; Cardin, V.; Yari, S. Can Internal Processes Sustain Reversals of the Ocean Upper Circulation? The Ionian Sea Example. *Geophys. Res. Lett.* **2010**, *37*, L09608. [CrossRef]
61. Gačić, M.; Civitarese, G.; Borzelli, G.L.E.; Kovačević, V.; Poulain, P.-M.; Theocharis, A.; Menna, M.; Catucci, A.; Zarokanellos, N. On the Relationship Between the Decadal Oscillations of the Northern Ionian Sea and the Salinity Distributions in the Eastern Mediterranean. *J. Geophys. Res.* **2011**, *116*, C12002. [CrossRef]
62. Gačić, M.; Civitarese, G.; Kovačević, V.; Ursella, L.; Bensi, M.; Menna, M.; Cardin, V.; Poulain, P.-M.; Cosoli, S.; Notarstefano, G.; et al. Extreme Winter 2012 in the Adriatic: An Example of Climatic Effect on the BiOS Rhythm. *Ocean Sci.* **2014**, *10*, 513–522. [CrossRef]
63. Theocharis, A.; Krokos, G.; Velaoras, D.; Korres, G. *An Internal Mechanism Driving the Alternation of the Eastern Mediterranean Dense/Deep Water Sources, in The Mediterranean Sea: Temporal Variability and Spatial Patterns 2014*; Borzelli, G.L.E., Ed.; American Geophysical Union/Wiley: Washington, DC, USA, 2014; Volume 202, pp. 113–137.
64. Placenti, F.; Torri, M.; Pessini, F.; Patti, B.; Tancredi, V.; Cuttitta, A.; Giaramita, L.; Tranchida, G.; Sorgente, R. Hydrological and Biogeochemical Patterns in the Sicily Channel: New Insights From the Last Decade (2010–2020). *Front. Mar. Sci.* **2022**, *9*, 733540. [CrossRef]
65. Gačić, M.; Schroeder, K.; Civitarese, G.; Cosoli, S.; Vetrano, A.; Borzelli, G.L.E. Salinity in the Sicily Channel Corroborates the Role of the Adriatic-Ionian Bimodal Oscillating System (BiOS) in Shaping the Decadal Variability of the Mediterranean Overturning Circulation. *Ocean Sci.* **2013**, *9*, 83–90. [CrossRef]
66. Goni, G.J.; Sprintall, J.; Bringas, F.; Cheng, L.; Cirano, M.; Dong, S.; Domingues, R.; Goes, M.; Lopez, H.; Morrow, R.; et al. More than 50 years of successful continuous temperature section measurements by the global expendable bathythermograph network, its integrability, societal benefits, and future. *Front. Mar. Sci.* **2019**, *6*, 452. [CrossRef]
67. Anderson, E.R. *Expendable Bathythermograph (XBT) Accuracy Studies*; NOSC Tech. Rep. 550; Naval Ocean System Center: San Diego, CA, USA, 1980; pp. 1–218.
68. Parras-Berrocal, I.M.; Vazquez, R.; Cabos, W.; Sein, D.V.; Álvarez, O.; Bruno, M.; Izquierdo, A. Dense water formation in the Eastern Mediterranean under global warming scenario. *EGUsphere* **2023**. *preprint*. [CrossRef]